Characterization of Ferromagnetic Saturation at 4.2K of Selected Bulk Rare Earth Metals for Compact High-Field Superconducting Cyclotrons

by

Mark A. Norsworthy

Submitted to the Department of Nuclear Science and Engineering
in partial fulfillment of the requirements for the degrees of
Master of Science in Nuclear Science and Engineering
and
Bachelor of Science in Nuclear Science and Engineering
at the
MASSACHUSETTS INSTITUTE OF TECHNOLOGY
June 2010

Signature of Author ....
Mark A. Norsworthy
Department of Nuclear Science and Engineering
May 24, 2010

Certified by..... .....
Timothy A. Antaya
Principal Research Engineer
Thesis Supervisor

Certified by..... .....
Jeffrey P. Freidberg
KEPCO Professor of Nuclear Science and Engineering
Thesis Reader

Accepted by..... .....
Jacquelyn C. Yanch
Professor of Nuclear Science and Engineering
Chair, Department Committee on Graduate Students

Characterization of Ferromagnetic Saturation at 4.2K of Selected Bulk Rare Earth Metals for Compact High-Field Superconducting Cyclotrons

by

Mark A. Norsworthy

Submitted to the Department of Nuclear Science and Engineering
on May 24, 2010, in partial fulfillment of the
requirements for the degrees of
Master of Science in Nuclear Science and Engineering
and
Bachelor of Science in Nuclear Science and Engineering

Abstract

The saturation magnetization of the rare earth ferromagnetic metals gadolinium and holmium was investigated. Cylindrical samples were placed in a superconducting test magnet and induced magnetic field measured at various applied fields. Data was obtained with Hall sensors mounted at the tips of the cylinders, and a powerful analytical calculation was derived to allow estimation of the saturation magnetization from this surface data. If the metal is saturated in a uniform, vertical magnetic field, the measured field at the surface due to the magnetization of the cylinder is just the saturation magnetization divided by a factor of two. Results show saturation magnetization values ranging from 0.5 to 1.5 T higher than iron, establishing the candidacy of these metals for advanced superconducting cyclotron pole tips.

Thesis Supervisor: Timothy A. Antaya
Title: Principal Research Engineer

Acknowledgments

I would like to express my deepest gratitude to Dr. Timothy Antaya for his guidance and support. He is both brilliant and kind, and it was a privilege to work with him.

I would also like to thank Dr. Makoto Takayasu, who provided not only the magnet and probe without which this experiment would have been impossible, but also his expert assistance and advice.

Further, I would like to acknowledge the expert machining performed by American Cryotech of Pelham, NH, whose precision work was exceptional and vital to the success of the project.

Finally, I thank my family, friends, and everyone in my life that has helped me get to where I am today. I am truly blessed and indebted to you all.

Table of Contents

1 Background

1.1 Historical Background of Cyclotron Particle Accelerators.....13

1.2 Long Range WMD Sensing Application and High Field Superconducting Cyclotrons 14

1.3 Ferromagnetism.....15

1.3.1 Rare Earth Ferromagnetic Materials.....16

2 Physics Basis for Measurement

2.1 Magnetic Induction of a Uniformly Magnetized Cylinder.....19

2.2 Modeling and Simulation.....22

3 Experiment Materials and Method

3.1 Materials.....26

3.2 Experimental Procedure.....29

4 Data and Results.....31

5 Discussion and Conclusion

5.1 Discussion.....36

5.2 Conclusion.....37

References.....39

Appendix A.....41

List of Figures

Figure 1, p. 16. Saturation magnetization of 1010 Steel. The saturation magnetization of a standard steel used in cyclotron poles is shown. 1010-steel saturates at $B_s = \mu_0 M_s = 2.05T$

Figure 2, p. 21. A right circular cylinder of an unknown ferromagnetic material, at saturation magnetization $\vec{M}_s$ is shown. We desire to determine the external field due to this magnetization along the z-axis outside the cylinder. The end face is assumed perpendicular to the z-axis.

Figure 3, p. 23. Output of Poisson software suite showing the coil dimensions of the 3 coils that constitute this air core 14T Oxford Superconducting Test Magnet. The geometry is symmetric rotationally about the vertical axis and has median plane symmetry about the x-axis.

Figure 4, p. 24. Output of Poisson software suite showing the magnet coil geometry with an iron sample in place, and current through the coils selected to yield a magnetic field at the origin with no sample of 4.24 T. The field at the origin with the iron sample in place is 6.27 T.

Figure 5, p. 27. Sample materials for experiment, from left to right: Stainless Steel rod, G-10 Dummy rod, Iron rod, and Gadolinium rod. Holmium is not shown.

Figure 6, p. 28. Photograph of top G-10 cap mounted to probe assembly with Hall sensor installed.

Figure 7, p. 28. Photograph of fully assembled test apparatus with G-10 dummy rod in place and both Hall sensors installed, prior to insertion in test magnet.

Figure 8, p.28. Photograph of fully assembled test apparatus with iron sample in place and both Hall sensors installed, prior to insertion in test magnet.

Figure 9, p. 32. A comparison of measured data with Poisson-simulated data. The vertical axis indicates the measured or simulated field at the tip of the sample, while the horizontal axis indicates the magnetic field generated by the Oxford test magnet set by computer or simulated at the origin. The top grouping of three lines represents data taken with the holmium sample in place, while the bottom grouping of three lines represents data taken with no sample (air core). The dashed lines indicate Poisson-simulated data. It can be seen that data from the top Hall sensor correspond much more closely to the simulated data than that from the bottom Hall sensor.

Figure 10, p. 33. All relevant measured data are presented here. The vertical axis indicates the measured field at the top of the sample, while the horizontal axis indicates the magnetic field generated by the Oxford test magnet set by computer. The lines correspond to data taken with the G-10 dummy, iron, gadolinium, and holmium samples in place. Notable features include the non-linear curve at low field for the metal samples, and the approach to linearity at high fields, with higher B values measured for Gd and Ho than for Fe.

List of Tables

Table 1, p. 34. Results of saturation magnetization calculation using Equation 8. The first column identifies the metal, the middle three columns identify the average difference between the field at the sample tip with the sample in place and the field at the sample tip with no sample (air core), and the final column indicates the resulting calculated value for B_s.

Table 2, p. 34. Final estimated ranges of the saturation magnetization of bulk gadolinium and holmium metal. Values calculated with Equation 8 and corrected by comparison with known and simulated saturation magnetizations of iron and holmium, respectively. See text for details.

Chapter 1

Background

1.1 Historical Background of Cyclotron Particle Accelerators

Ernest Lawrence filed a patent for the first cyclotron particle accelerator in 1932 [1]. Cyclotrons are characterized by a vertical magnetic field that confines particles to circular orbits within the machine. In the simplest cyclotrons, the vertical magnetic field is essentially uniform as a function of radius. As particles are accelerated (increase in energy), their orbit radii increase such that their orbit frequency is unchanged. When the particles reach the outer edge of the machine, they are extracted as a continuous beam. This type of cyclotron is only useful for non-relativistic particles. Relativistic effects (particularly mass increase with energy) destroy synchronization between the particle orbits and the radiofrequency (rf) fields that provide the acceleration, limiting these cyclotrons to final energies of 20 MeV or less. [2]

In the 1950s, Azimuthally-Varying-Field (AVF) cyclotrons were introduced, also known as isochronous cyclotrons. Isochronous cyclotrons use a radially increasing magnetic field to balance the relativistic mass increase, restoring constant orbit frequency. However, a positive field gradient results in a negative field index and vertical defocusing. To compensate for this, isochronous cyclotrons also vary the magnetic field azimuthally via the use of raised sectors on the face of the magnet poles, creating a "hill-and-valley" geometry. Some sectors are simple wedge shapes, but most modern isochronous cyclotrons employ spiral sectors, often Archimedean spirals. The azimuthal field varies approximately as the inverse of the pole gap distance, and spiral pole sectors result in alternating focusing and defocusing effects depending on whether the particle is entering or leaving a hill region. Thus, alternating spiral-shaped "hill-and-valley" sectors result in a strong net vertical focusing [2]. The focusing field provided by azimuthal variation is called "flutter."

By the 1980s, superconducting coil isochronous cyclotrons had been introduced. These machines operate at a high enough magnetic field that the iron used to construct their poles is fully saturated. Iron's saturation magnetization is about 2 T. The flutter field in a fully

saturated cyclotron is thus proportional to the changing gap spacing and the saturation magnetization of iron. Limitations exist on gap spacing, and the strength of the flutter field relative to the primary magnetic field of the superconducting coils limits the focusing that can be brought to bear on the particles as they are accelerated. In other words, the maximum primary magnetic field in an isochronous cyclotron is limited by the strength of the flutter field, and in turn by the saturation magnetization of iron. Most superconducting cyclotrons operate at or below 5.5 T peak field. Because high field cyclotrons are desirable for a variety of reasons to be discussed later, it is necessary to increase the strength of the flutter field.

1.2 Long Range WMD Sensing Application and High Field Superconducting Cyclotrons

One of the many potential applications of high-field superconducting cyclotron particle accelerators is active interrogation of fissile materials at long (of order 1 km) range. Active interrogation refers to a process in which target fissile materials are stimulated to undergo fission, and signature radiations are detected to enable material identification. Electron accelerators are often used in such applications as a source of charged particles, which either interrogate the target directly or impact a target to generate a beam of neutrons or photons. These electron accelerators, derived from X-ray radiotherapy machines, are relatively compact and simple to operate. However, accurate detection at such ranges requires electron beams at unprecedented energies (requiring much larger machine size) and intensities (generating lethal doses of radiation). Moreover, the accelerator needs to be small and dependable to be deployable in a real-world environment. Simultaneously achieving milliampere proton intensities at GeV energies in a single stage accelerator, of any kind, has never been achieved [3]. Accordingly, the Defense Threat Reduction Agency is funding basic research at the MIT Plasma Science and Fusion Center for the study of the feasibility of ambitious high energy, high intensity single-stage cyclotrons that would be ideal for many long standoff active interrogation concepts of operation. This experiment was part of that overall project.

The final energy of a particle accelerated in a cyclotron is a function of the magnetic field (acceleration per orbit) and the accelerator radius (total path length). Therefore, if high-

energy particles are desired from a cyclotron, higher fields or larger overall size are needed. A larger overall size would limit the use of such a cyclotron for active interrogation, so our research approach is to raise the field. When the average field is raised, correspondingly higher flutter field is necessary to maintain the axial focusing effect. One approach to increasing the flutter field is to use nested superconducting coils as pole sectors, while another approach is to develop pole sectors with higher saturation magnetization than iron. The nested coils option would be quite complicated (spiral shape) and difficult (large forces), while increasing the flutter field by using a different ferromagnetic material would enable simple scale-up from existing cyclotron designs.

1.3 Ferromagnetism

It is well known that some ferromagnetic rare-earth metals with low Curie temperatures have higher magnetic saturation values than iron. Rare earth metals and their magnetic properties have been studied since at least the 1950s [4] – [9]. It is thought that these materials can be used; however, data suitable for engineering use in benchmarked design codes do not exist. Much of the data available in the literature comes from single-crystal studies on rare-earth metals, for example [4]; this data is inadequate for engineering use, which would require significant quantities of bulk materials. A reliable analysis of the saturation magnetization of rare-earth metals such as holmium is therefore needed to allow the limits of superconducting cyclotron accelerators to be expanded to high field, high intensity designs.

The pole sector technique relies in part upon the ferromagnetic properties of iron. Ferromagnetic materials are characterized by microscopic magnetic dipoles that align with one another if the material is below a temperature called the Curie temperature, Tc; above Tc, thermal motion prevents spontaneous alignment. When placed in an applied magnetic field, the magnetic domains of ferromagnetic materials align with the field, resulting in a net contribution to the overall field strength. Thus, iron pole sectors in a cyclotron magnetize in the same direction as the field, up to a saturation value of ~2.05 T determined by the material properties of iron. Generally, if one designs a 5 T superconducting isochronous cyclotron accelerator, the 5 T field is composed of ~3 T from the magnet coils themselves and ~2 T

from the saturated iron pole sectors. A standard steel alloy used in cyclotrons is 1010-steel, with has a carbon content of 0.2%. The saturation magnetization of 1010-steel is shown in Figure 1.

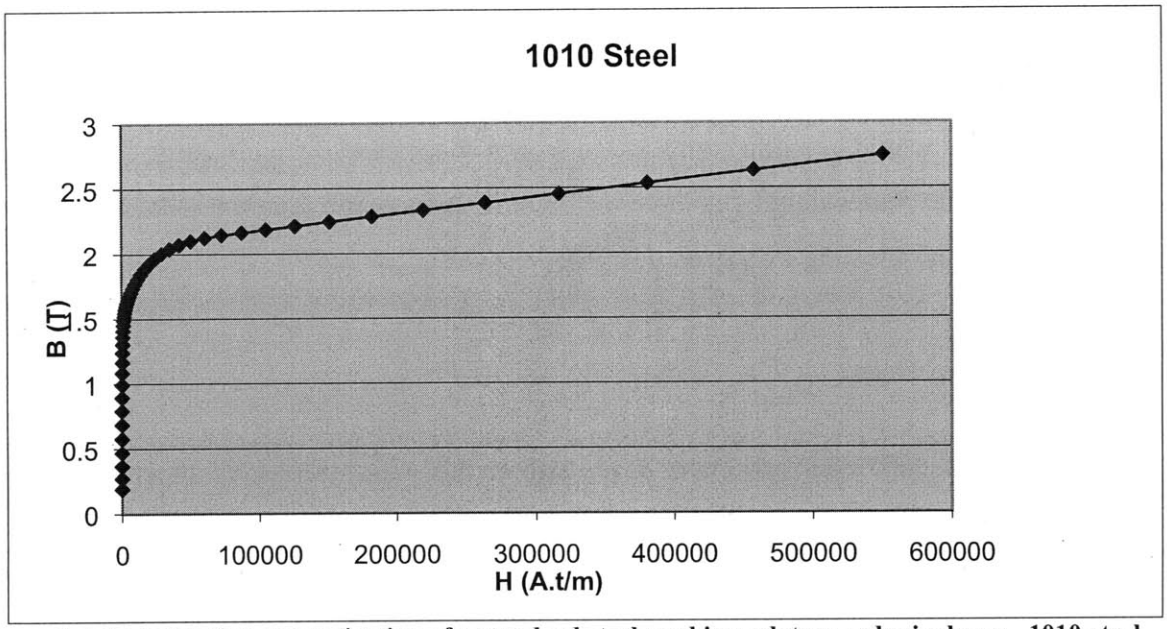

Figure 1. The saturation magnetization of a standard steel used in cyclotron poles is shown. 1010-steel saturates at $B_s = \mu_0 M_s = 2.05T$.

1.3.1 Rare Earth Ferromagnetic Materials

The most common ferromagnetic material is iron, but other materials exhibit ferromagnetism. The rare earth metals, elements with Z=57 to Z=71, are ferromagnetic but have Curie temperatures well below room temperature. Commonly seen neodymium permanent magnets are actually compounds of neodymium with transition metals that raise the Curie temperature above room temperature.

The strongest known elemental ferromagnet is holmium, with saturation magnetization listed in the literature as 3.9 T [10]. Holmium, however, is only ferromagnetic at extremely low temperatures (below 20 K), requiring the use of liquid helium to sufficiently cool the metal. Gadolinium is another interesting rare earth ferromagnetic material, because its Curie temperature is only slightly below room temperature (289 K). Gadolinium also saturates at a higher level than iron, but literature studies are often conducted on single crystals, or presented in outdated or hard-to-interpret units (ie, 7.05 Bohr magnetons/atom) [7].

Holmium has been successfully demonstrated as a magnetic flux concentrator in solenoid-type superconducting magnets, with stated field increases of ~3.5 T [10]. Holmium has also been demonstrated as a gradient enhancer in a quadrupole-type magnet [11]. Gadolinium is a less expensive rare-earth ferromagnet, and is produced in larger quantities annually worldwide. Both are candidate materials for superconducting cyclotron pole tips to enhance the flutter field, and are studied further in this experiment.

Chapter 2

Physics Basis for Measurement

2.1 Magnetic Induction of a Uniformly Magnetized Cylinder

We are interested in the determination of the saturated magnetization of rare earth ferromagnetic materials at low temperature. Our purpose is to use this material for poles in cyclotrons, replacing iron, which saturates at about 2 T, to extend the domain of isochronous cyclotrons to very high total magnetic fields (> 6 T) where they may become more compact. The high fields involved needed to magnetize these strong ferromagnetic materials precludes the use of a well-known technique, such as toroidal loop intrinsic magnetization measurement, where the fringe field effects in the source and sense coils would dominate the interpretation of the results. Instead, our experimental approach is to place cylindrical samples in the bore of a strong superconducting magnet that can generate bore magnetic inductions to 14 T, which should be sufficient to fully magnetize any ferromagnetic material to saturation. We then measure the total field in the bore of the magnet just outside of the magnetized cylinder and determine the saturation magnetization responsible for this total field (coil + magnetized sample). At low applied fields, where the sample ferromagnetic material is not fully magnetized, this technique would not work, due to the unknown and non-linear nature of the magnetization of the rare earth material. We claim that at saturation we can make this determination. The basis for that claim is presented here.

From Ampere's basic experimental law we can write the magnetic induction $\vec{B}$ due to a current distribution $\vec{J}(\vec{x})$ as

$$\vec{B}(\vec{x}) = \frac{\mu_0}{4\pi}\int \vec{J}(\vec{x}') \times \frac{\vec{x}-\vec{x}'}{\left[\vec{x}-\vec{x}'\right]^3} d^3\vec{x}' \qquad (1)$$

where the integral is over the 'primed' source terms. Consider the case of a uniformly magnetized right cylinder of a ferromagnetic material at saturation, whose symmetry axis is the z-axis and whose upper face is located at z=0, as shown in Figure 2. The magnetization

may be represented by a volume current density $\vec{J}_s$ having at each end a surface current σ_s given by

$$\sigma_s = \hat{n} \cdot \vec{J}_s \cos\theta = \mu_0 M_s \cos\theta = B_s \cos\theta \qquad (2)$$

where M_s is the saturation magnetization, $B_s = \mu_0 M_s$ and $\cos\theta$ is the angle between the upper unit normal and the z-axis. With Eq.(2) substituted into Eq.(1), and assuming $\hat{n} \| \hat{z}$, the volume integral reduces to a surface integral over faces of the cylinder.

$$\vec{B}_s(\vec{x}) = \frac{B_s}{4\pi} \oint \frac{\vec{x} - \vec{x}'}{\left[\vec{x} - \vec{x}'\right]^3} \cdot d\vec{a}' \qquad (3)$$

Eq. (3) tells us that the external field $\vec{B}_s$ due to the magnetization M_s anywhere in space is strictly due to an integral over all surfaces of the cylinder. For the field on the z-axis above the ends, the radial cylindrical surface does not contribute to Eq.(3), and we can always move the other end face far enough away that its contribution to the integral in Eq.(3) can be made small. Further, considering Figure 2, we may write $(\vec{x} - \vec{x}')$ for points located on the z-axis as $(z\hat{z} + \rho\hat{\rho})$ and $d\hat{a} = 2\pi\rho d\rho \hat{z}$, and the external induction due to M_s above the face at z=0 is then

$$B_1 = \frac{B_s z}{2} \int_o^a \rho d\rho / \left[\rho^2 + z^2\right]^{3/2} \qquad (4)$$

where a is the radius of the cylinder. This may be immediately evaluated to give

$$B_1 = \frac{B_s z}{2} \left[\frac{-1}{\sqrt{z^2 + \rho^2}} \right]_0^a = \frac{B_s}{2} \left[1 - \frac{1}{\sqrt{1 + a^2/z^2}} \right] \qquad (5)$$

At z=0 this reduces to the important result that

$$B_1(z=0) = B_s/2 \qquad (6)$$

meaning that the field at the surface due to the fully saturated ferromagnetic cylinder is just half of the saturation magnetization of the cylinder. Further, we observe also that in the limit as $z \to \infty$ that Eq.(5) properly goes to zero.

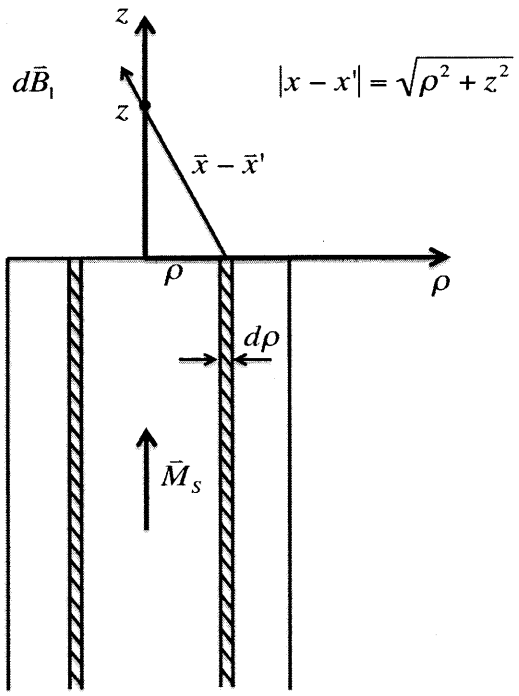

Figure 2. A right circular cylinder of an unknown ferromagnetic material, at saturation magnetization $\vec{M}_s$ is shown. We desire to determine the external field due to this magnetization along the z-axis outside the cylinder. The end face is assumed perpendicular to the z-axis.

To summarize, Eq.(5) gives us a method to determine the saturation magnetization of a cylindrical specimen, by measuring the field outside along the normal to the face. The assumptions in this measurement are only that:

(a) the sample be at saturation where the magnetization is then uniform,

(b) that the measurement be made normal to an end surface, and

(c) that the other end surface be sufficiently far away that its contribution at z is negligible.

or we would have to add an additional term of the same form but with opposite sign as compensation.

$$B_1 = \frac{B_s}{2}\left[1 - \frac{z}{\sqrt{z^2 + a^2}}\right] - \frac{B_s}{2}\left[1 - \frac{(z+L)}{\sqrt{(z+L)^2 + a^2}}\right] \qquad (7)$$

Where L is the length of the cylinder. At z=0, and using the dimensions of the samples used in this experiment, we find the result

$$B_1(z=0) \approx \frac{B_s}{2} * 0.996546 \qquad (8)$$

Equation 8 will be used in this experiment to estimate the saturation magnetization of samples of ferromagnetic rare earth metals.

2.2 Modeling and Simulation

To obtain data on the saturation magnetization of bulk rare-earth ferromagnetic materials, a method was devised in which bulk metal samples would be held in the magnetic field of a superconducting test magnet and the magnetic field (B) measured as a function of the applied field in the magnet (H). A 14-T liquid-He cooled superconducting test magnet (hereafter called the Oxford magnet) was available for use with the kind support of Dr. Makoto Takayashu.

A model for the magnet geometry was produced for use in the Poisson software program developed at Los Alamos National Laboratory (LANL). Magnet schematics were examined for coil number and dimensions, and trial values of coil currents were tested until a field strength and profile at magnet center were established that were consistent with the manufacturer's magnet documentation. The final coil geometry is shown in Figure 3.

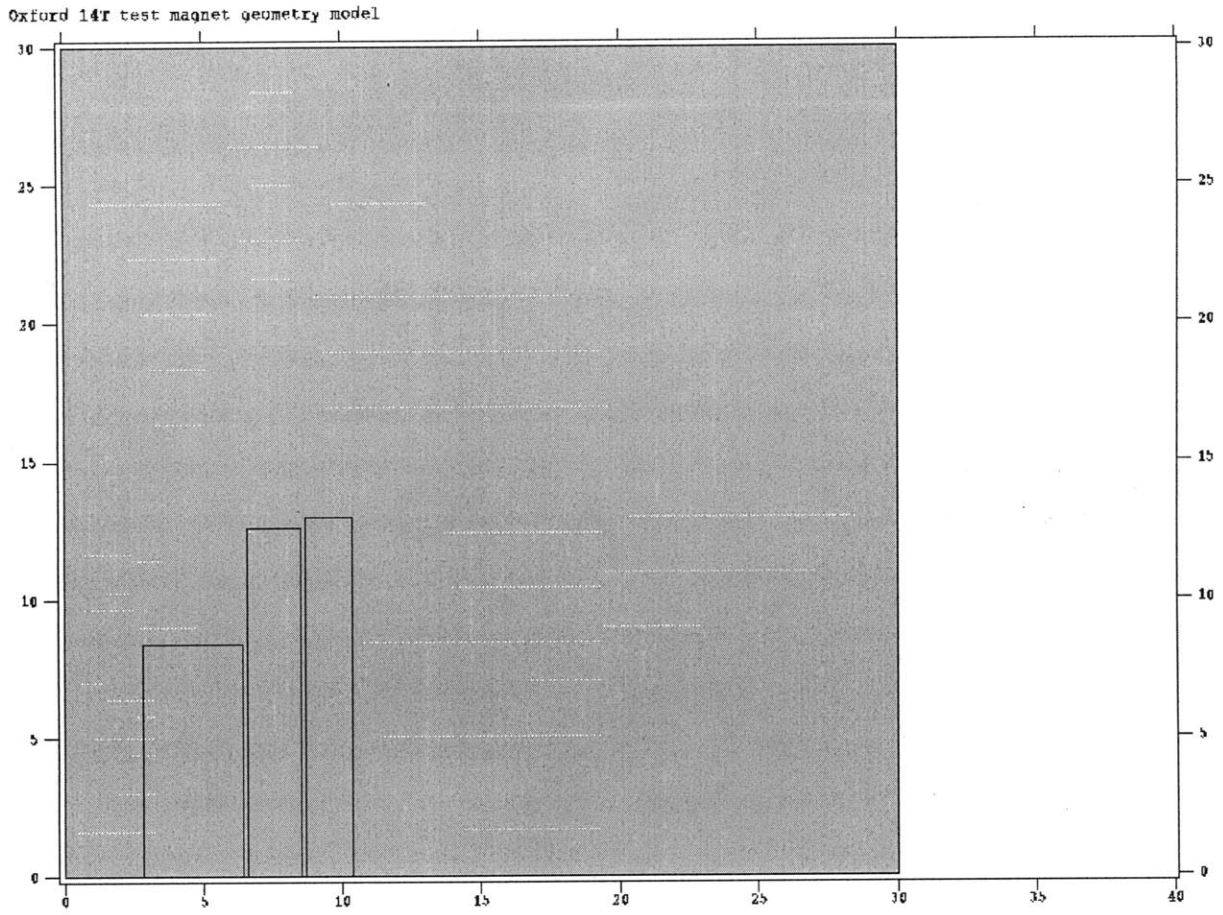

Figure 3. Output of Poisson software suite showing the coil dimensions of the 3 coils that constitute this air core 14T Oxford Superconducting Test Magnet. The geometry is symmetric rotationally about the vertical axis and has median plane symmetry about the x-axis.

Based on the bore of the magnet and coil spacing, sample dimensions were chosen to be right cylindrical rods 1" in diameter and 6" long. Poisson simulations were conducted with various current densities in the coils, and B_z values determined at the center and at the surface of the sample (or if no sample was present, at the center only). Iron magnetization data is available internally in the Poisson software, so the first set of simulations used iron as the sample material. A representative simulation is depicted in Figure 4.

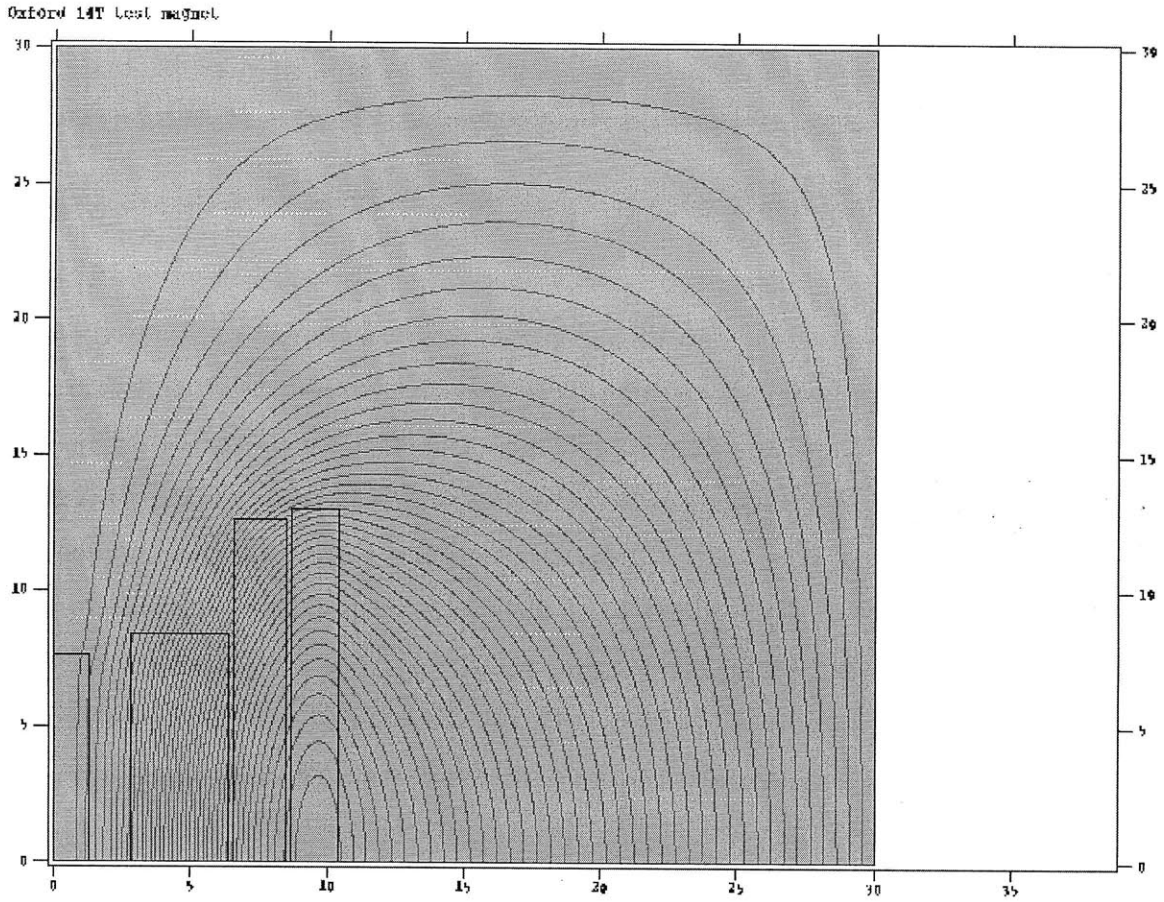

Figure 4. Output of Poisson software suite showing the magnet coil geometry with an iron sample in place, and current through the coils selected to yield a magnetic field at the origin with no sample of 4.24 T. The field at the origin with the iron sample in place is 6.27 T.

Saturation of the iron is clearly well simulated. With the same current through the coils, the measured field at the center with no sample was 4.24 T. With iron in place, the measured field at the center was 6.27 T, consistent with the ~2 .05T saturation magnetization of iron. Simulations at higher field showed linear increase in measured field with current, consistent with saturated material.

A table of B vs. H values was needed to simulate the magnetization of holmium using Poisson. A 1983 paper by Schauer and Arendt [10] provided a table of B and H values for holmium, for which a fit was generated using Matlab to generate sufficient points for a Poisson table. The values used in Poisson are given in Appendix A. Simulations were then performed using holmium samples instead of iron.

Chapter 3

Experiment Materials and Method

3.1 Materials

The metal samples used in the experiment were 1" diameter rods 6" in length of 99.9% pure iron, gadolinium, and holmium purchased from American Elements, Los Angeles, CA. The iron was purchased as a control sample, while gadolinium and holmium were purchased as the samples to be studied. A G-10 sample blank of the same dimensions was used to obtain direct measurements of the magnetic field generated by the Oxford test magnet. The sample blank included a 0.25" diameter cavity on the axis to accommodate a 0.25" diameter carbon steel rod. The G-10 and stainless steel combination was tested to verify the safety of the experiment design, particularly the ability of the sample holder caps to withstand any de-centering forces. There were some uncertainties concerning the ability of the magnet to withstand the applied loads, and the small, slightly magnetic carbon steel rod was used to verify the proper function of the Oxford magnet with a centered magnetic load in the bore.

Figure 5 shows, from left to right, the carbon steel rod, the G-10 sample blank, the iron rod, and the gadolinium rod. The holmium rod is not shown. The G-10 sample blank has a 0.25" diameter axial cavity that accommodates the carbon steel rod. Prior to the experiment the samples were kept under a nitrogen atmosphere to prevent oxidation. The photograph in Figure 5 was taken post-experiment and oxidation is visible on the gadolinium rod, probably due to condensation on the sample as it warmed up.

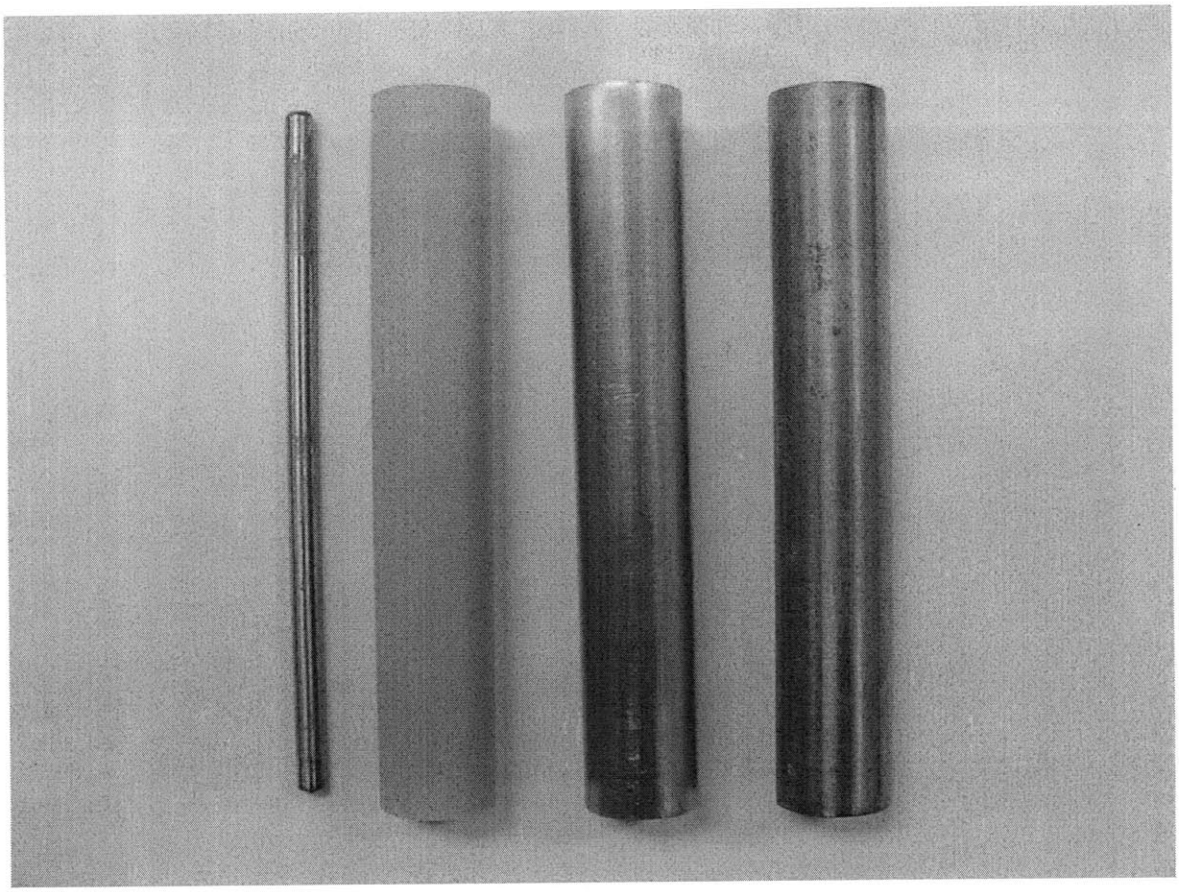

Figure 5. Sample materials for experiment, from left to right: Stainless Steel rod, G-10 Dummy rod, Iron rod, and Gadolinium rod. Holmium is not shown.

G-10 end caps were designed to mount the samples to an existing probe apparatus for the Oxford test magnet. The top and bottom caps were attached to the samples by six brass set screws equally spaced around the circumference, and the top cap included an axial tap for a 0.25" diameter brass threaded rod. The rod fit into the end of the existing apparatus and was secured by a brass nut and washer. The end caps contained precisely machined grooves to accommodate the cryogenic Hall probe sensors (model BHT-921). The sensors were purchased from Sypris Test and Measurement. Figures 6 through 8 show the Hall sensors, G-10 caps, and assembled caps and sample.

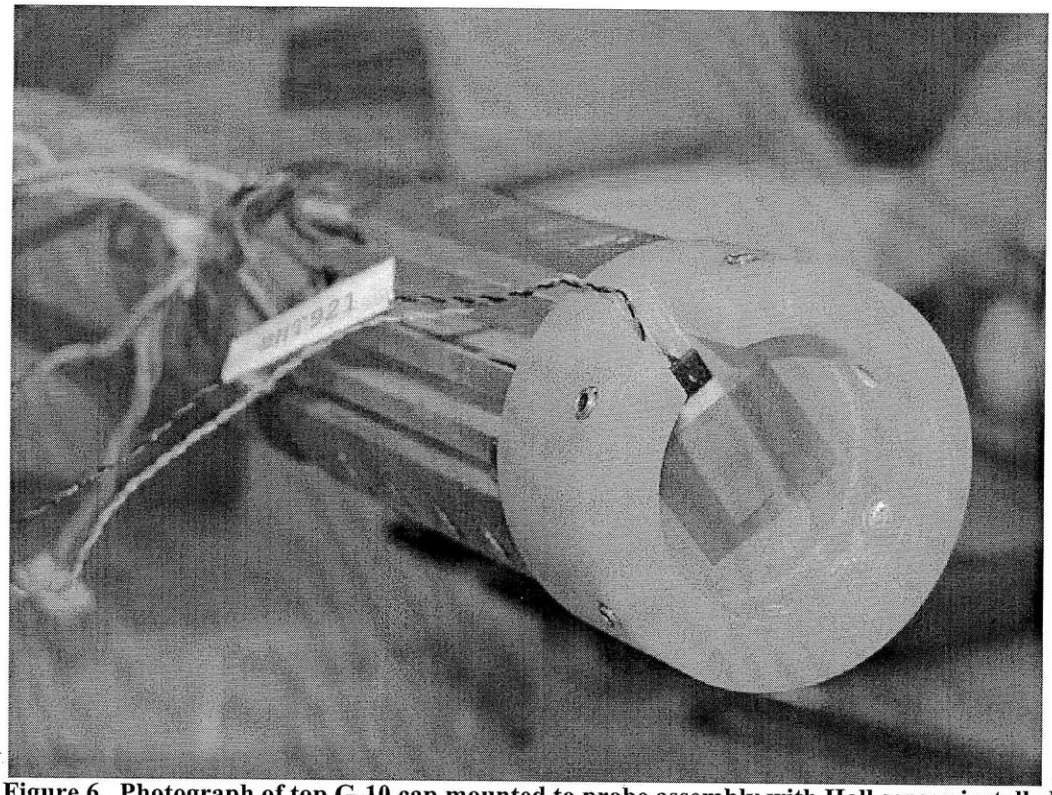

Figure 6. Photograph of top G-10 cap mounted to probe assembly with Hall sensor installed.

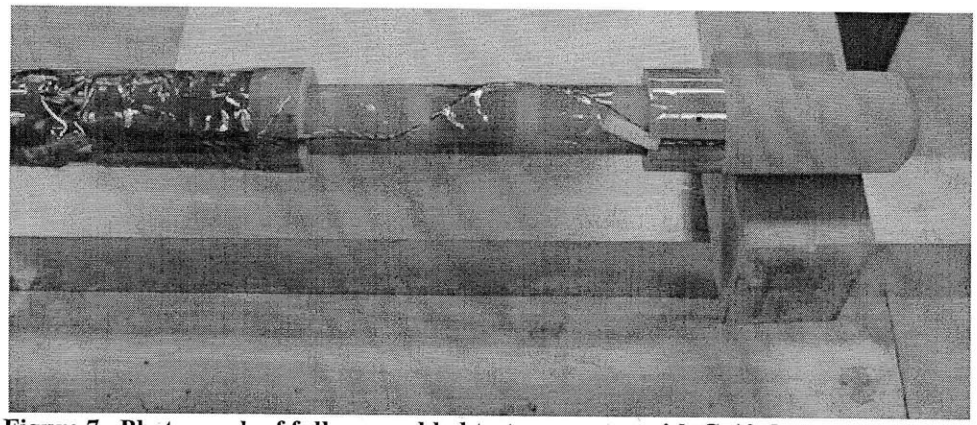

Figure 7. Photograph of fully assembled test apparatus with G-10 dummy rod in place and both Hall sensors installed, prior to insertion in test magnet.

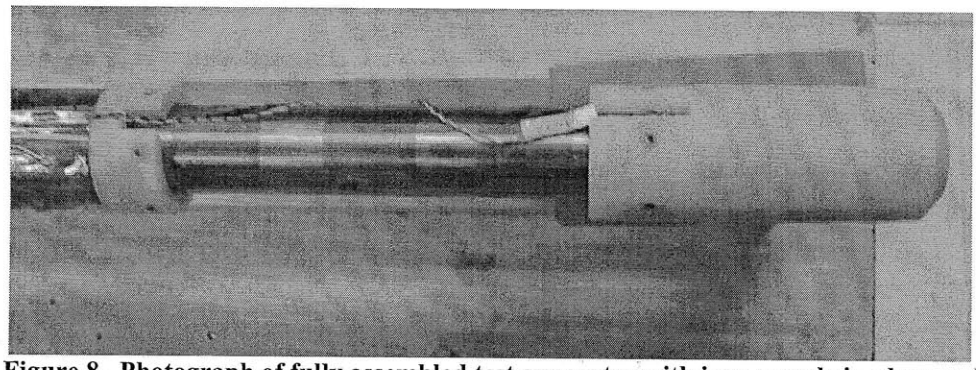

Figure 8. Photograph of fully assembled test apparatus with iron sample in place and both Hall sensors installed, prior to insertion in test magnet.

3.2 Experimental Procedure

The procedure for the experiment was to pre-cool the Oxford magnet with liquid nitrogen to 77K, remove the nitrogen and fill the magnet with liquid helium to bring the temperature to 4.2K. The end of the assembled probe was pre-cooled by immersion in liquid nitrogen for several minutes prior to insertion to remove most of the enthalpy of the materials. The probe was slowly inserted into the test magnet and secured, and at least ten minutes allowed to elapse to ensure the sample was fully cooled to 4.2 K. The hall probe leads were connected to wires that corresponded to pins on the top of the probe assembly, which in turn were connected to a constant current source and two voltmeters. The Oxford test magnet was controlled by a sophisticated, computer-controlled, intelligent power supply capable of regulating the current in the coils to milliamp precision. The current in the coils was increased to various set points corresponding to specific test magnetic inductions at the center of the magnet. The readings of the voltmeters, corresponding to the Hall Voltages of the two magnetic sensors, at each set point were recorded, and the current in the magnet reset to zero. At that point, the probe could be removed, warmed by means of heat guns, and the sample replaced with the next one.

Chapter 4

Data and Results

The voltage readings for the Hall sensors at the top and bottom of the sample were recorded at various increasing set values for the magnetic field at the center of the magnet. These voltage measurements were converted into field measurements using conversion factors provided with the Hall sensors (0.853 mV/kG for the top sensor and 0.860 mV/kG for the bottom sensor).

Figure 9 shows a comparison of the measured data using the non-magnetic G-10 dummy sample and the holmium sample to the simulated data generated using the Poisson magnet model. It can be seen that the top sensor's data agrees well with the simulation, while the bottom sensor's data is significantly different. It is thought that the source of this discrepancy could be the inherent difficulty in ensuring that the bottom sensor is centered in the magnet, due to the long lever arm to the end of the sample and the nature of the reinforcement in the composite bore tube of the magnet. Any misalignment would have a greater effect at the bottom sensor location. Based on this discrepancy, the remaining plots and analysis are based only on the data from the top Hall sensor.

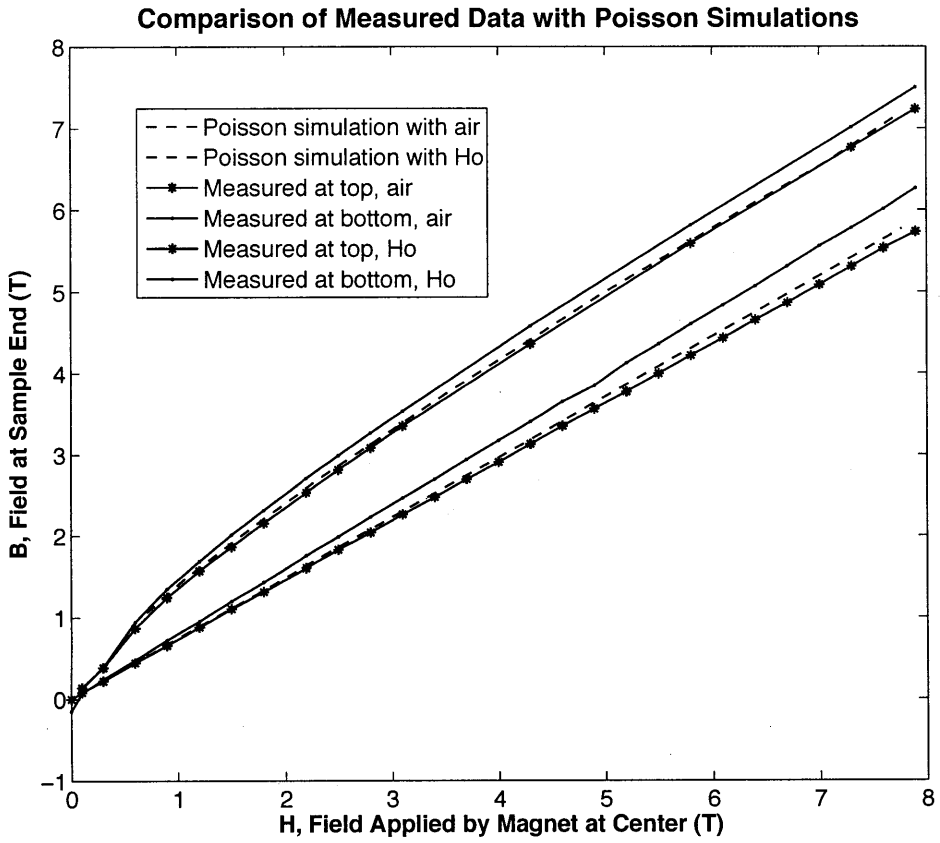

Figure 9. A comparison of measured data with Poisson-simulated data. The vertical axis indicates the measured or simulated field at the tip of the sample, while the horizontal axis indicates the magnetic field generated by the Oxford test magnet set by computer or simulated at the origin. The top grouping of three lines represents data taken with the holmium sample in place, while the bottom grouping of three lines represents data taken with no sample (air core). The dashed lines indicate Poisson-simulated data. It can be seen that data from the top Hall sensor correspond much more closely to the simulated data than that from the bottom Hall sensor.

It can be seen from Figure 9 that with the G-10 dummy sample in place the field at the tip increases linearly with the field at the center of the magnet. With the metal sample in place, the field increases rapidly as the metal magnetizes and asymptotically approaches linearity similar to that obtained with the dummy sample, indicating that the sample has reached saturation. By Eq.(6), at saturation, we expect at the hall sensors to measure an incremental field increase above the air core field of $B_s/2$, decreased slightly by the gap between the sensor and the sample pole face. As can be seen from Figure 9, holmium sample fields are more than 1T higher than the air core field of the magnet..

Measurement runs were conducted with each of the three metal samples. All data obtained are presented in Figure 10.

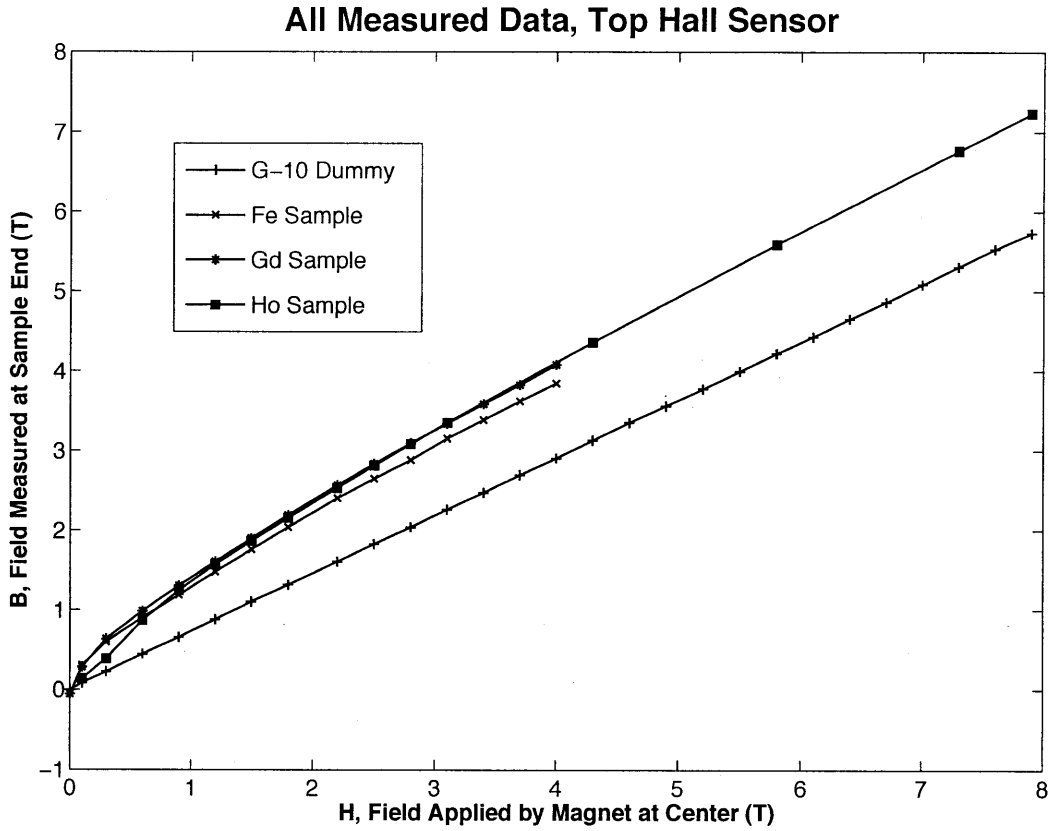

Figure 10. All relevant measured data are presented here. The vertical axis indicates the measured field at the top of the sample, while the horizontal axis indicates the magnetic field generated by the Oxford test magnet set by computer. The lines correspond to data taken with the G-10 dummy, iron, gadolinium, and holmium samples in place. Notable features include the non-linear curve at low field for the metal samples, and the approach to linearity at high fields, with higher B values measured for Gd and Ho than for Fe.

The measured data shown in Figure 10 was used to calculate the estimated saturation magnetization of the respective metals. The calculation was based on the two highest measured data points for each metal. The corresponding dummy sample measurements were subtracted, and the resulting two numbers averaged. This resulting average was then used in Equation 8 to calculate B_s, the saturation magnetization. The results for each metal are presented in Table 1, rounded to two significant digits.

Table 3. Results of saturation magnetization calculation using Equation 8. The first column identifies the metal, the middle three columns identify the average difference between the field at the sample tip with the sample in place and the field at the sample tip with no sample (air core), and the final column indicates the resulting calculated value for B_s.

Results and Calculated Saturation Magnetization, B_s

Metal	Difference 1	Difference 2	Average	Calculated B_s (T)
Fe	0.9379	0.9261	0.9320	1.87
Gd	1.1723	1.1313	1.1518	2.31
Ho	1.5006	1.4537	1.4771	3.01

To determine the error of the calculated value of B_s, two checks were performed. First, the calculated value for iron was compared to the known saturation magnetization of iron, 2.05 T. This check gives an error of -9.6%, indicating that the calculated values are somewhat low relative to the expected values. This is likely due to sensor positioning, the location of the samples in the magnet bore, and an unknown location of the actual Hall sensor in the senor package. The second check was to compare the calculated value for holmium with the Poisson-simulated saturation magnetization of holmium, 3.5 T. This check gives an error of -16.3%. Thus, we report final estimates for the saturation magnetization of gadolinium and holmium, based on our measured data, in Table 2.

Table 4. Final estimated ranges of the saturation magnetization of bulk gadolinium and holmium metal. Values calculated with Equation 8 and corrected by comparison with known and simulated saturation magnetizations of iron and holmium, respectively. See text for details.

Estimated Ranges for Saturation Magnetization of Gadolinium and Holmium

	Lower estimate (109% of calculated value)	Upper estimate (116% of calculated value)
Gadolinium	2.52 T	2.68 T
Holmium	3.28 T	3.49 T

Chapter 5

Discussion and Conclusion

5.1 Discussion

We have demonstrated a useful analytical calculation for the saturation magnetization of a fully saturated cylinder in a uniform magnetic field, and used that result to estimate the saturation magnetization of bulk metal samples of Fe, Gd, and Ho. The calculated results were shown to be low relative to the known and simulated saturation magnetizations of Fe and Ho. The discrepancy is easily explained, by noting the following points:

(a) The magnetic field applied by the Oxford test magnet was not exactly vertical with respect to the sample pole face, and the radial component results in edge effects that increase with the magnetic susceptibility of the sample.
(b) These edge effects were not taken into account in the idealized analytical calculation.
(c) The assumed value of $z = 0$ for the separation between the sensor and the sample is certainly too small. There was a gap, at minimum, of the thickness of the Kapton tape securing the sensor to the top G-10 cap. Any gap will reduce the measured value, but we expect this effect to be small in this experiment.

Thus we report ranges for the saturation magnetization of gadolinium and holmium based on measured data, corrected with the known saturation data for iron and the modeled saturation data for holmium.

We point out that the reported range for gadolinium is almost certainly still low, even with the aforementioned corrections, due to the fact that the highest applied central field for gadolinium was 4 T, as opposed to 7.9 T for holmium. A re-examination of the iron measured data, which also was stopped at 4 T applied, revealed that the iron only showed an approach to the same slope as the dummy sample data just at the end of the measurement run.

Furthermore, the gadolinium curve and holmium curve overlap almost exactly at 4 T, with the same slope, and are almost indistinguishable in Figure 10. This suggests that the reported range for gadolinium is low, and that bulk gadolinium may in fact saturate at a level closer to the reported values for bulk holmium. Further experimentation is necessary to determine the true saturation magnetization value for bulk gadolinium.

The goal of the experiment was to obtain saturation magnetization data on bulk holmium and gadolinium to determine their candidacy as cyclotron pole materials. The results show that holmium is definitely a candidate material, with a saturation magnetization 1.2 to 1.5 T higher than that of iron. The results for gadolinium show saturation only 0.5 to 0.7 T higher than iron, but we expect that the true value is higher, which would make it a candidate material as well.

Suggested further work would be to re-measure gadolinium at higher field. Refinement of the measurement method would consist of a new sample holder to more precisely hold the samples in the center of the magnet, which would include the fabrication of a new 4K bore tube for the magnet. Other measurement techniques, such as placing a sensor in the center of the sample, as opposed to the ends, would also be useful for validating these results, if the sensor can be installed without disrupting the properties of the sample too greatly.

5.2 Conclusion

We have defined a useful relation, Equation 6, for estimating the saturation magnetization of a ferromagnetic metal cylinder in a uniform vertical magnetic field based on the measured value at the surface. We developed a method for holding cylindrical samples in the center of a superconducting test magnet, and directly measured the magnetic field at the surface of metal samples at increasing applied magnetic fields. Finally, we used the measured data and the analytical relation to estimate the saturation magnetization for bulk samples of iron, gadolinium, and holmium, and determined that both gadolinium and holmium are candidate materials for the pole tips of advanced superconducting cyclotrons.

References

[1] E. O. Lawrence, "Method and Apparatus for the Acceleration of Ions," U.S. Patent 1,948,384, January 26, 1932.

[2] S. Humphries, *Principles of Charged Particle Acceleration*. Albuquerque, NM: John Wiley and Sons, 1999.

[3] T.A. Antaya, L. Bromberg, and J.V. Minervini, "Frontier Studies of Single State Superconducting Cyclotron-based Primary Accelerators for Topic I: Sensing Fissile Materials at Long Range (Thrust 1)," DTRA Basic Research Proposal, July 2008.

[4] H.E. Nigh, S. Legvold, and F.H. Spedding, "Magnetization and electrical resistivity of gadolinium single crystals," *Physical Review*, vol. 132, no. 3, pp. 1092-1097, November 1963.

[5] S. Legvold, F.H. Spedding, F. Barson, and J.F. Elliott, "Some magnetic and electrical properties of gadolinium, dysprosium, and erbium metals," *Reviews of Modern Physics*, vol. 25, no. 1, pp. 129-130, January 1953.

[6] J.F. Elliott, S. Legvold, and F.H. Spedding, "Some magnetic properties of gadolinium metal," *Physical Review*, vol. 91, no. 1, pp. 28-30, July 1953.

[7] W.E. Henry, "Magnetic moments and apparent molecular fields in some rare earth metals and compounds," *Journal of Applied Physics*, vol. 29, no. 3, pp. 524-525, March 1958.

[8] B.L. Rhodes, S. Legvold, F.H. Spedding, "Magnetic properties of holmium and thulium metals," *Physical Review*, vol. 109, no. 5, pp. 1547-1550, March 1958.

[9] S. Yu. Dan'kov, A.M. Tishin, V.K. Pecharsky, and K.A. Gschneidner, "Magnetic phase transitions and the magnetothermal properties of gadolinium," *Physical Review B*, vol. 57, no. 6, pp. 3478-3490, February 1998.

[10] W. Schauer and F. Arendt, "Field enhancement in superconducting solenoids by holmium flux concentrators," *Cryogenics*, pp. 562-564, October 1983.

[11] D.B. Barlow, R.H. Kraus, C.T. Lobb, M.T. Menzel, and P.L. Walstrom, "Compact high-field superconducting quadrupole magnet with holmium poles," *Nuclear Instruments and Methods in Physics Research*, vol. A313, pp. 311-314, 1993.

Appendix A

Sample Poisson Input File

The file below generates an applied field at center of 8 T (determined by setting the sample region material to 1, for air). As listed below, the sample is holmium, and the program uses the long table of B and H values immediately following the outer coil section to perform its calculation. The values were generated using fits to data in Schauer and Arendt, 1983 [10].

```
Oxford 14T test magnet external table
Vers. 0 TAA, MAN 2010

; Copyright 2010, Massachusetts Institute of Technology
; Unauthorized commercial use is prohibited.

&reg kprob=0,           ; Poisson or Pandira problem
mode=0,                 ; Use internal table for material 2
mat=1,                  ; First region is material air
nbslo=1,                ; Neumann boundary condition on lower edge
nbsup=0,                ; Dirichlet boundary condition on upper edge
nbslf=0,                ; Dirichlet boundary condition on left edge
nbsrt=0,                ; Dirichlet boundary condition on right edge
icylin=1,               ; cylindrical symmetry
ienergy=1,              ; calculate the stored energy
iverg=100,        ; first convergence test at 100 iterations
;ktop=60,                ; Field interpolation at 4 points along X
;ltop=3,                 ; Field interpolation at 3 points along Y
;xminf=0,xmaxf=12.5,     ; X range for field interpolation
;yminf=0,ymaxf=0.5,      ; Y range for field interpolation
dx=0.1 &                ; X mesh size for problem and dy set off dx

&po x=0.,y=0. &         ; Entire geometry is air, initially
&po x=30.,y=0. &        ; dimensions in cm
&po x=30.,y=30. &
&po x=0.,y=30. &
&po x=0.,y=0. &


&reg mat=2, mtid=7 mshape=0 & ; mat=2 turns on iron, mtid=7 changes to Ho
&po x=0.,y=0. &               ; sample region
&po x=1.27,y=0. &
&po x=1.27,y=7.62 &
&po x=0.,y=7.62 &
&po x=0.,y=0. &


&reg mat=1,cur=3.4e5 &     ; inner coil
&po x=2.8,y=0. &
&po x=6.4,y=0. &
&po x=6.4,y=8.4 &
&po x=2.8,y=8.4 &
```

```
&po x=2.8,y=0. &

&reg mat=1,cur=2.26667e5 &      ; middle coil
&po x=6.6,y=0. &
&po x=8.5,y=0. &
&po x=8.5,y=12.6 &
&po x=6.6,y=12.6 &
&po x=6.6,y=0. &

&reg mat=1,cur=2.26667e5 &      ; outer coil
&po x=8.7,y=0. &
&po x=10.4,y=0. &
&po x=10.4,y=13. &
&po x=8.7,y=13. &
&po x=8.7,y=0. &

&mt mtid=7
BH=0  0
4924.598953 25
6692.538094 275
8439.895637 525
10147.96104 775
11798.02729 1025
13376.06284 1275
14881.92873 1525
16318.05451 1775
17686.86972 2025
18990.80393 2275
20232.28667 2525
21413.74751 2775
22537.61599 3025
23606.32166 3275
24622.29407 3525
25587.96278 3775
26505.75734 4025
27378.10729 4275
28207.44218 4525
28996.19158 4775
29746.78502 5025
30461.64762 5275
31142.86033 5525
31791.92074 5775
32410.26997 6025
32999.3491  6275
33560.59924 6525
34095.46147 6775
34605.3769  7025
35091.78663 7275
35556.13175 7525
35999.85336 7775
36424.39255 8025
36831.19042 8275
37221.68808 8525
37597.32661 8775
37959.54711 9025
38309.79069 9275
38649.49843 9525
38980.11144 9775
```

39303.07064 10025
39619.58064 10275
39930.14399 10525
40235.13339 10775
40534.92156 11025
40829.88122 11275
41120.38509 11525
41406.80588 11775
41689.51632 12025
41968.8891 12275
42245.29697 12525
42519.11262 12775
42790.70879 13025
43060.45818 13275
43328.73351 13525
43595.9075 13775
43862.35287 14025
44128.44233 14275
44394.5486 14525
44661.0444 14775
44928.30237 15025
45196.60668 15275
45465.97848 15525
45736.39035 15775
46007.81483 16025
46280.2245 16275
46553.59189 16525
46827.88958 16775
47103.09012 17025
47379.16607 17275
47656.08998 17525
47933.83441 17775
48212.37193 18025
48491.67508 18275
48771.71643 18525
49052.46854 18775
49333.90395 19025
49615.99524 19275
49898.71495 19525
50182.03565 19775
50465.92989 20025
50750.37024 20275
51035.32924 20525
51320.77945 20775
51606.69344 21025
51893.04377 21275
52179.80298 21525
52466.94364 21775
52754.4383 22025
53042.25953 22275
53330.37988 22525
53618.7719 22775
53907.40816 23025
54196.26122 23275
54485.30362 23525
54774.50794 23775
55063.84672 24025
55353.29253 24275

55642.81792 24525
55932.39545 24775
56300.94144 25100
57381.07658 26100
58461.21171 27100
59541.34685 28100
60621.48198 29100
61701.61712 30100
62781.75225 31100
63861.88739 32100
64942.02252 33100
66022.15766 34100
67102.29279 35100
68182.42793 36100
69262.56306 37100
70342.6982 38100
71422.83333 39100
72502.96847 40100
73583.1036 41100
74663.23874 42100
75743.37387 43100
76823.50901 44100
77903.64414 45100
78983.77928 46100
80063.91441 47100
81144.04955 48100
82224.18468 49100
83304.31982 50100
84384.45495 51100
85464.59009 52100
86544.72523 53100
87624.86036 54100
88704.9955 55100
89785.13063 56100
90865.26577 57100
91945.4009 58100
93025.53604 59100
94105.67117 60100
95185.80631 61100
96265.94144 62100
97346.07658 63100
98426.21171 64100
99506.34685 65100
100586.482 66100
101666.6171 67100
102746.7523 68100
103826.8874 69100
104907.0225 70100
105987.1577 71100
107067.2928 72100
108147.4279 73100
109227.5631 74100
110307.6982 75100
111387.8333 76100
112467.9685 77100
113548.1036 78100
114628.2387 79100
115708.3739 80100

```
116788.509  81100
117868.6441 82100
118948.7793 83100
120028.9144 84100
121109.0495 85100
122189.1847 86100
123269.3198 87100
124349.455  88100
125429.5901 89100
126509.7252 90100
127589.8604 91100
128669.9955 92100
129750.1306 93100
130830.2658 94100
131910.4009 95100
132990.536  96100
134070.6712 97100
135150.8063 98100
136230.9414 99100
137311.0766 100100
138391.2117 101100
139471.3468 102100
140551.482  103100
141631.6171 104100
142711.7523 105100
143791.8874 106100
144872.0225 107100
145952.1577 108100
147032.2928 109100
148112.4279 110100
149192.5631 111100
150272.6982 112100
151352.8333 113100
152432.9685 114100
153513.1036 115100
154593.2387 116100
155673.3739 117100
156753.509  118100
157833.6441 119100
158913.7793 120100
159993.9144 121100
161074.0495 122100
162154.1847 123100 &
```